Journal of Nuclear Medicine, published on July 13, 2019 as doi:10.2967/jnumed.119.230565

Total-Body Dynamic Reconstruction and Parametric Imaging on the uEXPLORER

Running title: Total-Body Parametric Imaging

Authors: Xuezhu Zhang[1], Zhaoheng Xie[1], Eric Berg[1], Martin S. Judenhofer[1], Weiping Liu[2], Tianyi Xu[2], Yu Ding[2], Yang Lv[2], Yun Dong[2], Zilin Deng[2], Songsong Tang[2], Hongcheng Shi[3], Pengcheng Hu[3], Shuguang Chen[3], Jun Bao[2], Hongdi Li[2], Jian Zhou[1], Guobao Wang[4], Simon R. Cherry[1,4], Ramsey D. Badawi[1,4], and Jinyi Qi[1]

Affiliations: [1]Department of Biomedical Engineering, University of California, Davis, CA, USA;

[2]United Imaging Healthcare, Shanghai, China;

[3]Zhongshan Hospital, Fudan University, Shanghai, China

[4]Department of Radiology, University of California Davis Medical Center, CA, USA

First author: Xuezhu Zhang, Department of Biomedical Engineering, University of California, Davis. One Shields Avenue, Davis, CA 95616 USA E-mail: zhang@ucdavis.edu

Corresponding author: Jinyi Qi, Department of Biomedical Engineering, University of California, Davis. One Shields Avenue, Davis, CA 95616 USA E-mail: qi@ucdavis.edu

Word count: 5000

Financial support:

This work was supported in part by the National Institutes of Health under Grant R01 CA206187.

ABSTRACT

Rationale: The world's first 194-cm long total-body PET/CT scanner (uEXPLORER) has been built by the EXPLORER consortium to offer a transformative platform for human molecular imaging in clinical research and healthcare. Its total-body coverage and ultra-high sensitivity provide opportunities for more accurate tracer kinetic analysis in studies of physiology, biochemistry and pharmacology. The objective of this study is to demonstrate the capability of total-body parametric imaging and to quantify the improvement in image quality and kinetic parameter estimation by direct and kernel reconstruction of the uEXPLORER data.

Methods: We developed quantitative parametric image reconstruction methods for kinetic analysis and used them to analyze the first human dynamic total-body PET study. A healthy female subject was recruited and a one-hour dynamic scan was acquired during and following an intravenous injection of 256 MBq of ^{18}F-FDG. Dynamic data were reconstructed using a 3D TOF list-mode OSEM algorithm and a kernel-based algorithm with all quantitative corrections implemented in the forward model. The Patlak graphical model was used to analyze the FDG kinetics in the whole body. The input function was extracted from a region over the descending aorta. For comparison, indirect Patlak analysis from reconstructed frames and direct reconstruction of parametric images from the list-mode data were obtained for the last 30 min of data.

Results: Images reconstructed by OSEM show good image quality with low noise, even for the 1-s frames. The image quality was further improved by using the kernel method. Total-body Patlak parametric images were obtained by using either indirect estimation or direct reconstruction. The direct reconstruction method was found to improve parametric image quality with better contrast versus background noise tradeoff compared to the indirect method with a 2-3 fold variance reduction. The kernel-based indirect Patlak method offered similar image quality as the direct Patlak with less computation time and faster convergence.

Conclusion: This study demonstrated the capability of total-body parametric imaging using the uEXPLORER. Furthermore, the results showed the benefits of kernel-regularized reconstruction and direct parametric reconstruction – both can achieve superior image quality for tracer kinetic studies compared to the conventional indirect OSEM for total-body imaging.

Key Words: Positron emission tomography; tracer kinetics; total-body parametric imaging; kernel method; direct reconstruction

INTRODUCTION

Positron emission tomography (PET) has been widely used in oncology, neurology and cardiology by providing sensitive molecular imaging of biological processes using radiotracers (*1*). By means of dynamic acquisition over time, PET can measure the spatiotemporal distribution of radiotracers *in vivo,* which can be used to provide assays of physiologically and biologically relevant information, such as cerebral blood volume, blood flow, glucose metabolism, oxygen utilization, DNA synthesis, signal transduction, immune system activation, cancer cell phenotyping for molecularly targeted therapies, pharmacokinetics, pharmacodynamics, etc., through mathematical modeling of the tracer kinetics (*2*). Due to the limited length of current clinical PET scanners (e.g. typically covering an axial field-of-view (AFOV) of 15~30 cm), most dynamic PET scans in the past have been restricted to a single-bed scan over a limited region of the human body at one time. To acquire whole-body dynamic imaging (e.g. typically from head or neck to upper thigh), multi-bed scans (step-and-shoot or continuous-bed-motion) with a sequential multi-pass protocol were introduced to cover the body (*3,4*). However, two major drawbacks exist in the multi-bed multi-pass approach: 1) the temporal sampling resolution is limited due to the multi-bed acquisition and it is impossible to capture fast tracer dynamics except for a single body region; 2) the scan duration is divided among multiple bed positions, resulting in reduced sensitivity and a low signal-to-noise ratio (SNR) for parametric imaging.

To overcome the limitation of low sensitivity and short AFOV of current clinical PET scanners, the EXPLORER consortium has been developing very large AFOV imaging systems to offer a transformative platform for biomedical research and clinical applications (*5*). To date, the consortium has built a 45-cm long PMT-based (photomultiplier tube) PET (mini-EXPLORER-I) for non-human primate imaging (*6*), a 48-cm long SiPM-based (silicon photomultiplier) PET (mini-EXPLORER-II) for veterinary medical imaging (*7*), a scalable 70-cm long digital SiPM PET (PennPET EXPLORER) for torso imaging (*8*), and the recently completed 194-cm long PET/CT (uEXPLORER) [1] for total-body imaging (*9*). Compared to conventional scanners, the massively increased sensitivity of the uEXPLORER improves PET image quality through a high SNR that supports high spatial and temporal resolution that is also predicted to provide much better lesion detection capability and region-of-interest

[1] uEXPLORER is the product name of the 194-cm PET/CT built by the United Imaging Healthcare and we use it to referred to the specific scanner used in this paper.

(ROI) quantification performance (*10,11*). Its entire-body coverage and ultra-high sensitivity provide opportunities for more accurate tracer kinetic analysis in studies of human physiology, biochemistry and pharmacology. The uEXPLORER provides the first opportunity to obtain dynamic imaging of the entire body of an adult human with simultaneous coverage of all organs, tissues and cells throughout the body. The blood input function can also be extracted from the aorta or left ventricle, thus alleviating the need for invasive blood sampling, provided that metabolite activity is negligible over the time of the imaging study. The high sensitivity of the uEXPLORER also permits high-quality parametric imaging on the voxel level for the whole body, which can better model heterogeneous regional tracer kinetics than ROI-based analysis.

Parametric image reconstruction methods have been developed for linear graphical models (e.g. Patlak plot and Logan plot) and compartmental models (*12*). The conventional approach is to reconstruct the dynamic temporal frames first, and then fit the time-activity curves of each voxel with a kinetic model. This approach is commonly referred to as the indirect method. It is easy to implement, but usually results in high noise in the parametric images because the noise distribution in reconstructed images is difficult to model (*13*). Penalized maximum-likelihood image reconstruction methods can be used to improve the indirect parametric images (*14*). Regularization using kernel-based methods have also been developed to enhance the dynamic PET reconstruction by incorporating anatomic or dynamic features in the reconstruction through a kernel matrix (*15-17*). A better alternative to the indirect method is direct parametric reconstruction, which estimates the tracer kinetic parameters directly from the dynamic PET sinograms, because noise in PET sinograms can be accurately modeled. It has been shown that direct reconstruction methods can improve the image quality and SNR of parametric images (*18-20*).

In this work, we aimed to demonstrate the first total-body parametric imaging on a human subject using the uEXPLORER scanner and the performance improvement by using the kernel reconstruction and direct reconstruction in comparison with indirect reconstruction. In this first study, we focus on the linear Patlak graphical model, which has been widely studied to analyze the accumulation and retention of ^{18}F-FDG-6-PO$_4$ that occurs in proportion to the rate of glycolysis in specific tissues (*21*). For comparison, we study the indirect Patlak method based on either OSEM reconstruction or kernel reconstruction and also the direct Patlak reconstruction using the nested algorithm (*22*). The contrast versus noise curve was evaluated for the resulting parametric images to quantify the gain in noise reduction by the kernel regularization and direct parametric reconstruction.

MATERIALS AND METHODS

Scanner Description

The uEXPLORER scanner has an axial field of view of 194 cm and a transaxial field of view of 68.6 cm (*9*). It is constructed with 8 axial unit rings (each with an AFOV of 24 cm) formed from 24 detector modules with an inner ring diameter of 78.6 cm. Each module consists of 5×14 detector blocks with an array of 7×6 lutetium-yttrium oxyorthosilicate (LYSO) scintillator crystals. Each crystal has dimensions of 2.76×2.76×18.1 mm^3. The uEXPLORER has time-of-flight (TOF) capability with a system timing resolution of ~430 ps and energy resolution of 11.7% (*7*). A summary of the uEXPLORER's physical characteristics is provided in Table 1. The maximum difference of (±) 4 unit rings was in used in the fully 3D data acquisition with a maximum axial acceptance angle of ±57°. A unit-difference dependent coincidence time window was implemented (*11*), ranging from 4.5 ns for a unit difference of 0 to 6.9 ns for unit difference of ±4. The maximum ring difference of 4 unit rings was based on a previous simulation *(23)*, which showed that the noise-equivalent-count-rate reaches the peak with a maximum acceptance angle of ~55°. Due to the attenuation effect of an adult human body, only 1% prompts from the body are rejected at this maximum acceptance angle.

Quantitative Image Reconstruction and Correction

We developed quantitative image reconstruction software for the EXPLORER scanner (*24*). A TOF list-mode iterative reconstruction method was used to take advantage of the statistical and physical models of the PET imaging process. We modeled the system response by combining a calculated system matrix and a measured blurring kernel (*25*). The image-domain point spread function (PSF) was estimated by reconstructing simulated point sources at 11,532 transaxial and axial locations over the FOV. A component-based normalization was performed using a 2-meter long water cylinder phantom to estimate the crystal efficiencies and plane efficiency (*26*). The attenuation correction factors were obtained from a co-registered CT scan acquired using the CT component of the scanner. A Monte-Carlo multiple-scatter simulation technique was implemented on graphics processing unit (GPU) to provide scattered coincidence estimation (*27*). For random coincidence correction, the delayed coincidence method was used. Deadtime correction was not included in this initial study. Due to the huge number of lines-of-response (LOR) in this scanner (>90 billion before accounting for TOF), TOF sinograms are impractical to store. Instead, a block-based TOF sinogram is used to reduce the storage size of scatter and random sinograms (*24*). For each unit pair, we

grouped one transaxial block and two axial blocks to form 7×12 crystals as one element, and the resulting compressed TOF sinogram has 77 radial bins, 60 angular bins, 7×7 block ring pairs, and 27 TOF bins (273 ps wide). We interpolated the scatter and random mean from the compressed TOF sinogram for the list-mode image reconstruction (*24*).

Evaluation Studies

Human Subject Study. The first human dynamic total-body PET study was conducted on the uEXPLORER. A healthy female subject was recruited (61-yrs old, height 156 cm, weight 56 kg) and gave informed consent under the guidance of the Ethics Board of Zhongshan Hospital (Shanghai, China). A one-hour dynamic scan was performed immediately after an intravenous injection of 256 MBq of ^{18}F-FDG via a vein near the ankle. A total of ~61 billion prompt coincidences and ~41 billion delayed coincidences were recorded. The random fraction (*RF*) ranged from 63% to 70% during the acquisition time due to the changes in the tracer distribution and radioactive decay (Fig. 1A). To exploit the high temporal resolution of this scanner, we divided the dataset into 187 temporal frames: 60×1 s, 30×2 s, 20×3 s, 12×10 s, 50×30 s, and 15×120 s.

Comparison Study. For quantitative image reconstruction, corrections (normalization, attenuation, randoms, scatters, and resolution model) were implemented in the forward model. Dynamic data were reconstructed using the OSEM algorithm (Ordered Subset Expectation Maximization) and a kernel-based algorithm (kernel-EM). We used three composite frames (early 10 min, mid 20 min, and late 30 min) to extract image features for constructing the kernel matrix (*15*). Images were reconstructed into 239×239×679 matrix with 2.85-mm cubic voxels. The linear Patlak graphical method was adopted to analyze the FDG kinetics in different tissues using the last 30-min of data (*21*). For comparison, indirect Patlak analysis from the reconstructed frames and direct reconstruction using the nested algorithm (*22*) were conducted. The input function was extracted from a region of interest (ROI) placed over the descending aorta instead of the left ventricle to minimize blurring effects due to cardiac motion and spillover from the myocardium. Because we did not know the ground truth for the value of K_i (net influx rate) in each voxel, we quantified the performance using a contrast versus noise curve in two different body regions. The first one was in the brain, where the contrast was measured between the grey and white matter, and noise was calculated as the standard deviation of the pixels within a uniform ROI in the white matter. The second one was in the thorax, where

we measured the contrast of a focal region of uptake in the collarbone and the noise was calculated using the same white matter ROI. The high uptake in the collarbone was confirmed by a delayed scan acquired at 4-h post injection (*9*).

RESULTS

Dynamic Image Reconstruction

OSEM Reconstruction. The counting rate as a function of time from the ^{18}F-FDG dynamic scan on the human subject is shown in Fig. 1A. The total prompt rate (including trues, scatters, randoms) reached its peak value of 27.9 mcps (million counts per second) at 6 s after injection as the radiotracer travelled to the heart and then gradually dropped as the tracer distributed throughout the body, roughly following the decay of ^{18}F. Fig. 1B shows the anterior view of the maximum intensity projection (MIP) of OSEM reconstructed images of six selected temporal frames: five early 1-s frames from 17 s to 21 s and the last 2-min frame at 60 min. These dynamic images show good image quality with low noise, even for the 1-s frames. From the high temporal resolution dynamic images, we can clearly see tracer bolus entering the left ventricle first and then being pumped into the aorta. The temporal delay of the tracer bolus within the arterial tree is also evident.

Image-Derived Arterial Input Function. We extracted the time-activity-curves (TAC) from five blood regions (left ventricle, aorta, carotid artery, brachial artery, and femoral artery) and four major organs/tissues (myocardium, liver, grey matter, and white matter). The results in Fig. 2 show that the left ventricle is the earliest ROI to reach its peak value. The measured time delay between the left ventricle and aorta is about 1 to 2 s, and the time delay between the aorta and brachial and femoral arteries is about 5 s. The arterial curves measured from carotid, brachial and femoral arteries have lower peak values than that of the aorta due to dispersion and partial volume effects. The TACs in the ROIs of grey matter and white matter are very smooth, but not the ROIs in the myocardium and liver due to cardiac motion and respiratory motion. Based on motion and partial volume considerations, the ROI over the aorta was selected for all parametric analysis.

- *Kernel-EM Reconstruction*. Fig. 3 show MIPs of three composite images of early 10-min, mid 20-min and late 30-min scans, which have very low noise due to the large number of acquired counts (11.3, 20.2 and 28.6 billion prompts, respectively). These three composite images were used to calculate the kernel matrix using a Gaussian

function for the kernel-EM reconstruction (*15*). Fig. 4 shows the comparison of orthogonal slices between OSEM and kernel-EM reconstructions at two selected early frames (25-26 s and 60-62 s). We can see that the image quality of these short temporal frames was greatly improved by using the kernel method with enhanced contrast between organs and reduced noise in uniform regions.

Parametric Imaging

Indirect OSEM vs Kernel-EM vs Direct Reconstruction. Total-body parametric images were obtained by using the indirect parametric estimation based on either the OSEM or kernel-EM images, and by direct parametric reconstruction. Fig. 5A show the orthogonal slices of the Patlak K_i (slope of the Patlak plot) images. Due to the increased sensitivity of uEXPLORER, even the OSEM indirect method can generate high-quality Patlak images. In comparison, the kernel-EM indirect Patlak and direct Patlak reconstruction further improve the parametric image quality, with better contrast versus background noise tradeoff, over the indirect method. There is excellent delineation of the smaller structures in cerebral, cardiac and vertebral regions. The high spatial resolution images were reconstructed without incurring a high noise penalty. These observations are consistent with the quantitative results shown below.

ROI Quantification. Fig. 5B shows the K_i contrast between the grey matter and white matter vs. the standard deviation (STD) trade-off. It shows that the indirect OSEM Patlak (blue curve) has the highest noise level at the same K_i contrast ratio. Both the indirect kernel-EM and direct OSEM Patlak can achieve high image contrast with reduced noise. The indirect kernel-EM also has a fast convergence speed with much shorter reconstruction time compared to the direct OSEM Patlak. Fig. 5C shows the contrast versus noise curve for the focal uptake in the collarbone. The relative performance between the different methods remains the same with the kernel-EM and direct reconstruction achieving lower noise at the same contrast level than the indirect OSEM reconstruction.

SUV vs Patlak Slope. Fig. 6 shows the MIPs of the total-body SUV (late 30 min) and Patlak K_i images using different methods. We can see some correlation between SUV and Patlak K_i, but the Patlak K_i images have better tissue contrast without the interference of blood vessels. Furthermore, we also include a delayed scan of the same patient at 4-h post injection, which confirms the high focal uptake in the right sternoclavicular joint (Fig. 7). This result suggests that it may be possible to use parametric images to improve lesion conspicuity without the inconvenience of late time-point scanning.

DISCUSSION

Parametric imaging from dynamic PET has the benefit of improving the accuracy of tracer kinetic assays of biological and pharmacologic processes, which can only be inferred indirectly from static uptake PET images. In this work, we demonstrated total-body parametric imaging on the uEXPLORER scanner.

A major advantage of using the uEXPLORER is the simultaneous total-body coverage. Dynamic PET imaging using existing whole-body scanners is often limited to one-bed position, which is incompatible with the standard whole-body imaging protocol. While the multi-bed multi-pass approach can provide dynamic imaging with an extended AFOV, its temporal resolution is limited due to bed motion and sensitivity of the scanner, and it cannot capture fast tracer dynamics (e.g. total body perfusion with a highly diffusible tracer). Accurately tracking the time information of the bed motion is also required to obtain consistent results for parametric images (*4*). In contrast, the uEXPLORER scanner allows dynamic imaging of the entire body with high-temporal resolution because there is no bed motion and the system has high sensitivity to yield a high SNR in short time frames. With its total-body coverage, the uEXPLORER scanner simplifies the protocol for dynamic PET and every scan can be performed in a dynamic fashion without any sacrifice in the axial coverage. The total-body coverage also allows the image-derived arterial input function (AIF) to be determined from the aorta regardless of the organ of interest, which is impossible to perform on an existing whole-body PET except for regions near the heart. While it was expected that the AIF will be dependent on the sampling position, simultaneously measuring AIF at various sampling sites has not been possible due to the limited axial coverage of current clinical whole-body PET scanners. Using the uEXPLORER, we measured AIFs simultaneously from different sites inside the human body. The results show differences between the AIFs. Considering motion and partial volume effects, we chose the AIF from the aorta for all parametric analysis. Finding a way to use the AIFs from different arteries synergistically for total-body parametric imaging is an ongoing area of research.

Another major advantage of total-body dynamic imaging is the high sensitivity. Either with the step-and-shoot or continuous-bed-motion mode, the whole-body multi-bed multi-pass approach loses sensitivity for photon detection and misses spatiotemporal information between passes. Total-body dynamic PET can significantly improve the counting statistics because all organs are inside the FOV during the entire scan. The combination of

the total-body coverage and high sensitivity allows dynamic imaging with much higher temporal resolution than possible on existing PET scanners. High temporal resolution will be especially beneficial when nonlinear or more complex kinetic models are used.

There are a few limitations in this current work. Firstly, we focused on the Patlak graphical plot in our initial total-body parametric analysis due to its simplicity. This linear model is limited to irreversible tracer uptake, which can only represent the biologic behavior of certain organ (tissues & cells) and specific tracers. In many cases we need to investigate nonlinear kinetic models. This is an ongoing and future effort. Secondly, our preliminary human study only recruited a healthy volunteer. It is necessary to conduct patient studies in the future to evaluate the benefits and potential of parametric imaging in oncologic studies. Thirdly, due to the long scan duration, subject motion was observed in the dynamic images. To achieve accurate quantitation, motion correction is required. We are currently developing motion correction methods either as a post processing technique or in a motion-compensated reconstruction framework.

CONCLUSION

We have successfully demonstrated total-body parametric imaging on a human subject using the uEXPLORER scanner. In doing so we evaluated the benefits of kernel reconstruction and direct reconstruction methods in image quality of parametric images. With its total-body coverage and high sensitivity, the uEXPLORER scanner allows us to realize the full quantitative potential of PET imaging.

DISCLOSURE & ACKNOWLEDGEMENTS

RDB and SRC have a research agreement funded by United Imaging Healthcare. UC Davis also has a uEXPLORER sales-based gift agreement with United Imaging Healthcare. This work was supported in part by the National Institutes of Health under Grant R01 CA206187. No other potential conflicts of interest relevant to this article exist.

We acknowledge the contributions of all team members from UC Davis, United Imaging Healthcare and Zhongshan Hospital. We thank Dr. Terry Jones and Dr. Michael Phelps for their helpful comments on the manuscript. We thank Dr. Lorenzo Nardo for the confirmation of the high uptake region in the SUV images.

KEY POINTS:

QUESTION: The objective of this study is to demonstrate the capability of total-body parametric imaging and the improvement in image quality and kinetic parameter estimation by direct and kernel reconstruction of the uEXPLORER data.

PERTINENT FINDINGS: The reconstructed total-body parametric images show high image quality. The image quality can be further improved by using kernel-based regularization and direct parametric image reconstruction.

IMPLICATIONS FOR PATIENT CARE: With its total-body coverage and high sensitivity, the uEXPLORER allows us to realize the full quantitative potential of PET imaging.

REFERENCES

1. Phelps ME. Positron emission tomography provides molecular imaging of biological processes. *Proc Natl Acad Sci.* 2000;97:9226-9233
2. Cherry SR, Sorenson J, Phelps ME. Tracer kinetic modeling. In: *Physics in Nuclear Medicine*, 3rd Edition. Philadelphia, PA: Saunders/ Elsevier Health Sciences; 2003;377-403
3. Rahmim A, Lodge MA, Karakatsanis NA, et al. Dynamic whole-body PET imaging: principles, potentials and applications. *Eur J Nucl Med Mol Imaging*. 2019;46:501-518
4. Hu J, Panin V, Smith AM, et al. Clinical whole body CBM parametric PET with flexible scan modes. *IEEE Nuclear Science Symposium and Medical Imaging Conference* 2017;1-4
5. Cherry SR, Jones T, Karp JS, Qi J, Moses WW, Badawi RD. Total-body PET: maximizing sensitivity to create new opportunities for clinical research and patient care. *J Nucl Med.* 2018;59:3-12
6. Berg E, Zhang X, Bec J, et al. Development and evaluation of mini-EXPLORER: a long axial field-of-view PET scanner for non-human primate imaging. *J Nucl Med.* 2018;59:993-998
7. Lyu Y, Lv X, Liu W, et al. Mini EXPLORER II: a prototype high-sensitivity PET/CT scanner for companion animal whole body and human brain scanning. *Phys Med Biol*. 2019;64:075004
8. Karp J, Schmall J, Geagan M, et al. Imaging performance of the PennPET Explorer scanner. *J Nucl Med.* 2018;59(S1):222
9. Badawi RD, Shi H, Hu P, et al. First human imaging studies with the EXPLORER total-body PET scanner. *J Nucl Med*. 2019;60:299-303
10. Surti S, Karp JS. Impact of detector design on imaging performance of a long axial field-of-view, whole-body PET scanner. *Phys Med Biol*. 2015;60:5343–5358
11. Zhang X, Badawi RD, Cherry SR, Qi J. Theoretical study of the benefit of long axial field-of-view PET on region of interest quantification. *Phys Med Biol.* 2018;63:135010
12. Carson RE. Tracer kinetic modeling in PET. In: Bailey DL, Townsend DW, Valk PE, Maisey MN, eds. *Positron Emission Tomography*. New York, NY: Springer; 2005;127-159
13. Tsoumpas C, Turkheimer FE, Thielemans K. Study of direct and indirect parametric estimation methods of linear models in dynamic positron emission tomography. *Med Phys.* 2008;35:1299-1309

14. Yang L, Wang G, Qi J. Theoretical analysis of penalized maximum-likelihood Patlak parametric image reconstruction in dynamic PET for lesion detection. *IEEE Trans Med Imaging*. 2016;35:947-956
15. Wang G, Qi J. PET image reconstruction using kernel method. *IEEE Trans. Med. Imag.* 2015;34:61-71
16. Zhang X, Zhou J, Wang G, et al. Feasibility study of micro-dose total-body dynamic PET imaging using the EXPLORER scanner. *J Nucl Med*. 2014;55(S1):269
17. Gong K, Cheng-Liao J, Wang G, Chen KT, Catana C, Qi J. Direct Patlak reconstruction from dynamic PET data using the kernel method with MRI information based on structural similarity. *IEEE Trans Med Imaging*. 2018;37:955-965
18. Yan J, Planeta-Wilson B, Carson RE. Direct 4-D PET list mode parametric reconstruction with a novel EM algorithm. *IEEE Trans Med Imag.* 2012;31:2213-2223
19. Wang G, Qi J. Direct estimation of kinetic parametric images for dynamic PET. *Theranostics*. 2013;3:802–815
20. Reader AJ, Verhaeghe J. 4D image reconstruction for emission tomography. *Phys Med Biol*. 2014;59:R371-418
21. Patlak CS, Blasberg RG. Graphical evaluation of blood-to-brain transfer constants from multiple-time uptake data. generalizations. *J Cereb Blood Flow Metab*. 1985;5:584-590
22. Wang G, Qi J. Acceleration of the direct reconstruction of linear parametric images using nested algorithms. *Phys Med Biol*. 2010;55:1505–1517
23. Zhang X, Badawi RD, Cherry SR, Qi J. Total-body parametric imaging using the EXPLORER. *IEEE Nuclear Science Symposium and Medical Imaging Conference* 2018;TBPI MIC-WS2 II: 3024
24. Zhang X, Zhou J, Cherry SR, Badawi RD, Qi J. Quantitative image reconstruction for total-body PET imaging using the 2-meter long EXPLORER scanner. *Phys Med Biol.* 2017;62:2465–2485
25. Zhou J, Qi J. Efficient fully 3D list-mode TOF PET image reconstruction using a factorized system matrix with an image domain resolution model. *Phys Med Biol*. 2014;59:541-559
26. Tang S, Zhao Y, Fan X, Wang J, Dong Y. Normalization for long axial field-of-view, whole-body PET scanner by continuously moving acquisition. *IEEE Nuclear Science Symposium and Medical Imaging Conference* 2018;TBPI MIC-WS2 II:3011

27. Ding Y, Lv Y, Deng Z, Yang G, Hu D, Dong Y. Distributed reconstruction architecture of uEXPLORER. *IEEE Nuclear Science Symposium and Medical Imaging Conference* 2018;TBPI MIC-WS2 II:3015

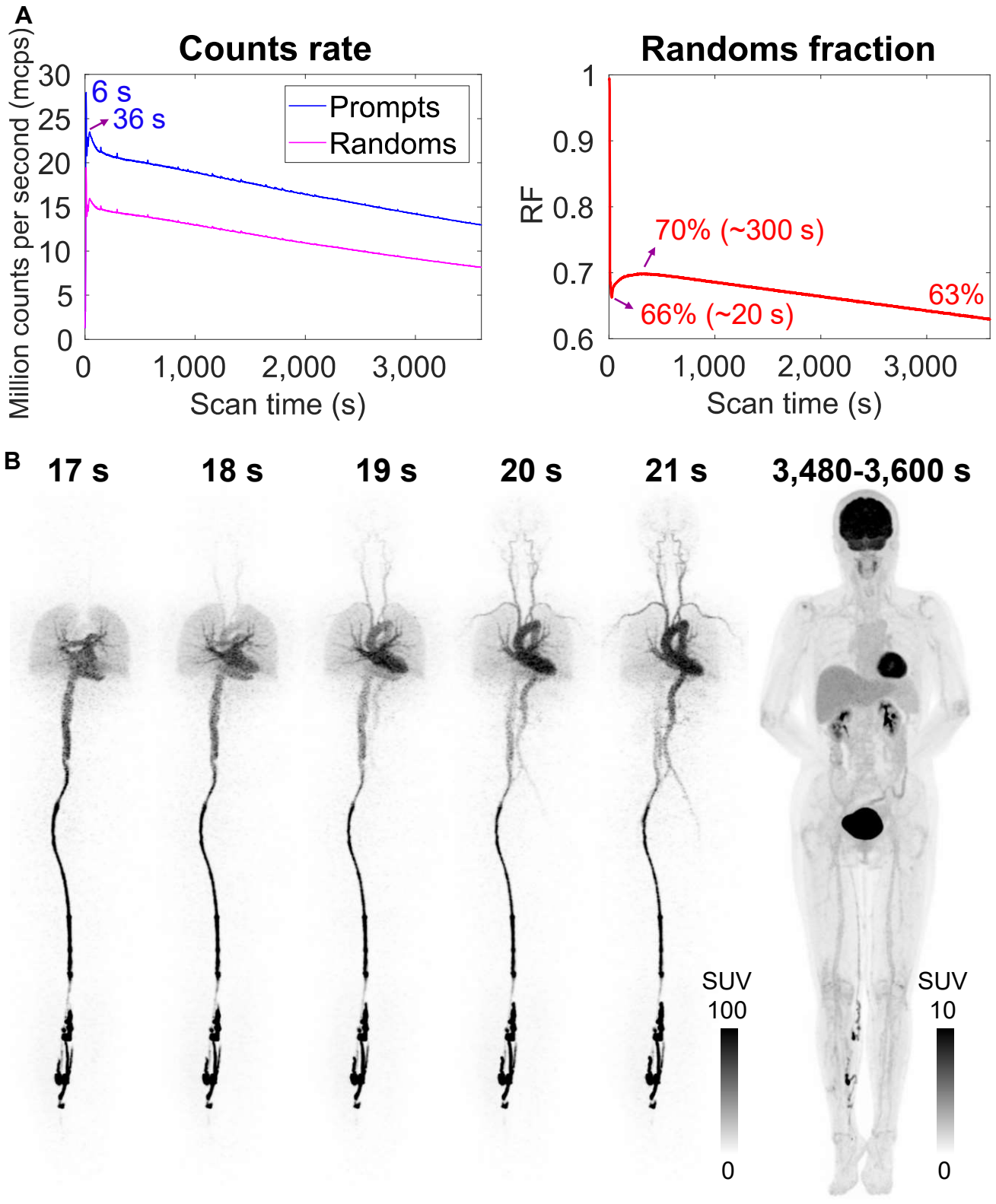

FIGURE 1. (A) Count rate and random fraction of 1-h ^{18}F-FDG dynamic scan of the human subject. (B) Maximum intensity projection (MIP) of selected dynamic OSEM reconstructed images (1-s and 120-s frames). The SUV images are shown in inverse gray scale with the maximum set to 100 and 10, respectively.

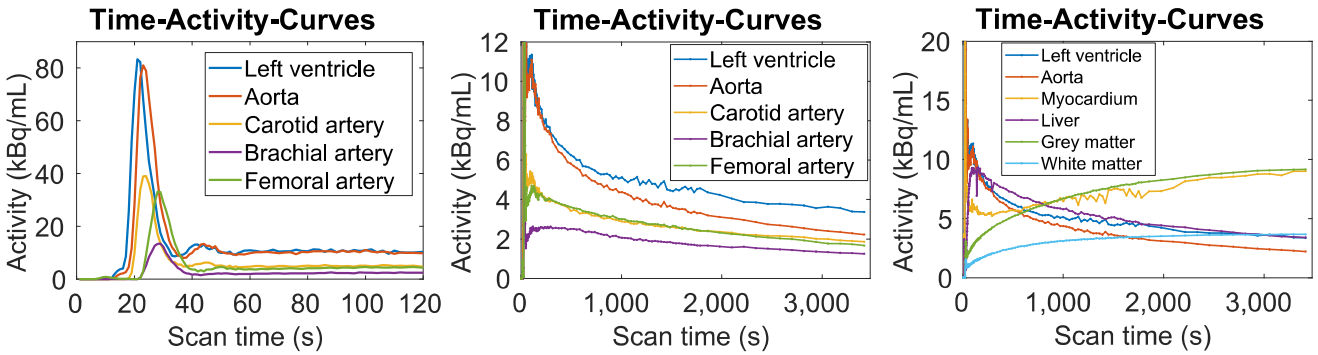

FIGURE 2. OSEM image-derived ROI-based blood input functions and major organs/tissues time activity curves. (left): Arterial input functions from different ROIs during the first 2 min; (middle): Arterial input functions during the whole 1-h scan zoomed in on 0-12 kBq/mL scale; (right) Time activity curves of major organs/tissues of interest.

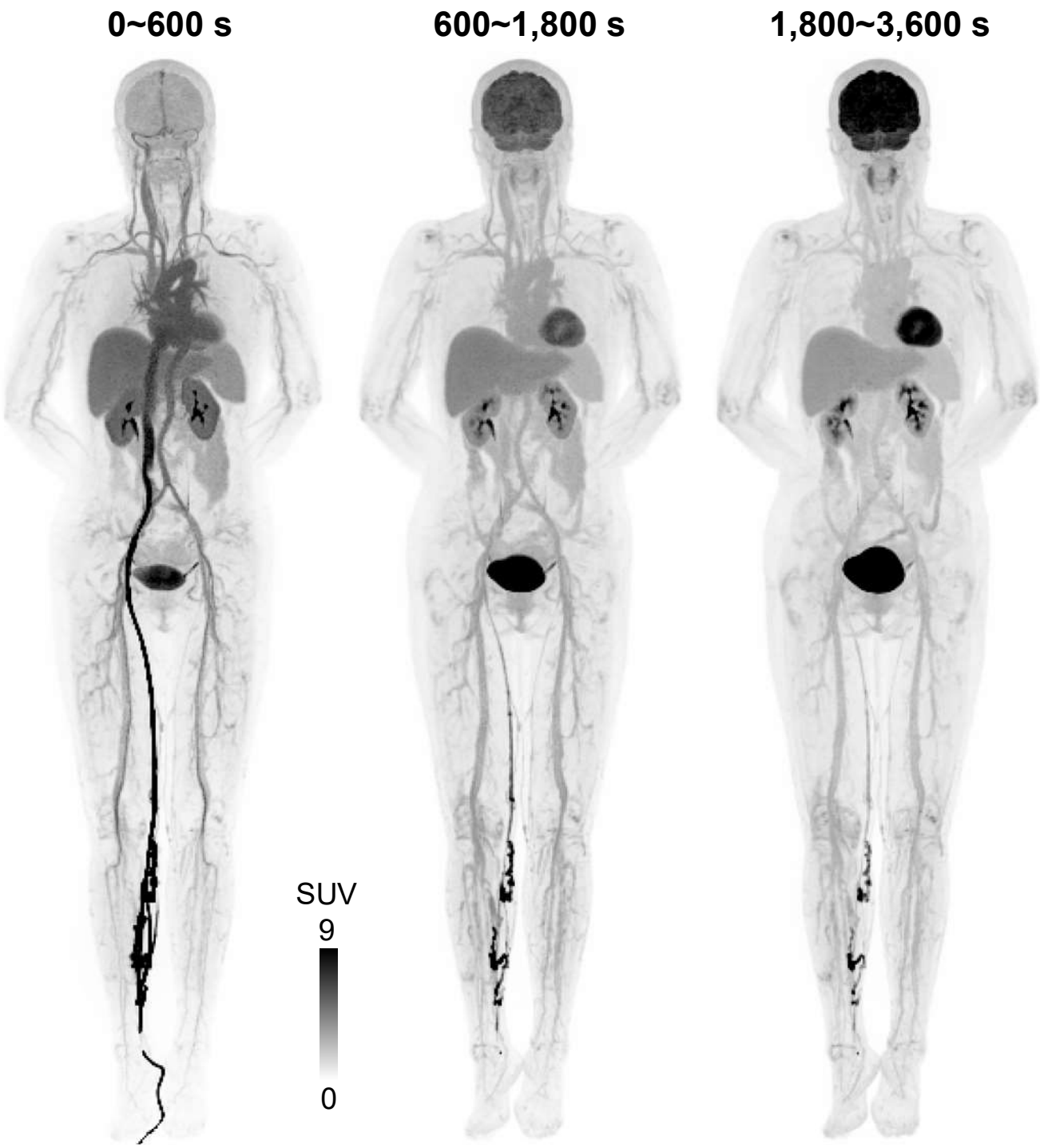

FIGURE 3. Reconstructed dynamic composite SUV images (OSEM MIP) of early 10-min, mid 20-min, late 30-min scans. The images were used to extract features to construct the kernel matrix. The SUV images are shown in inverse gray scale with the maximum set to 9.

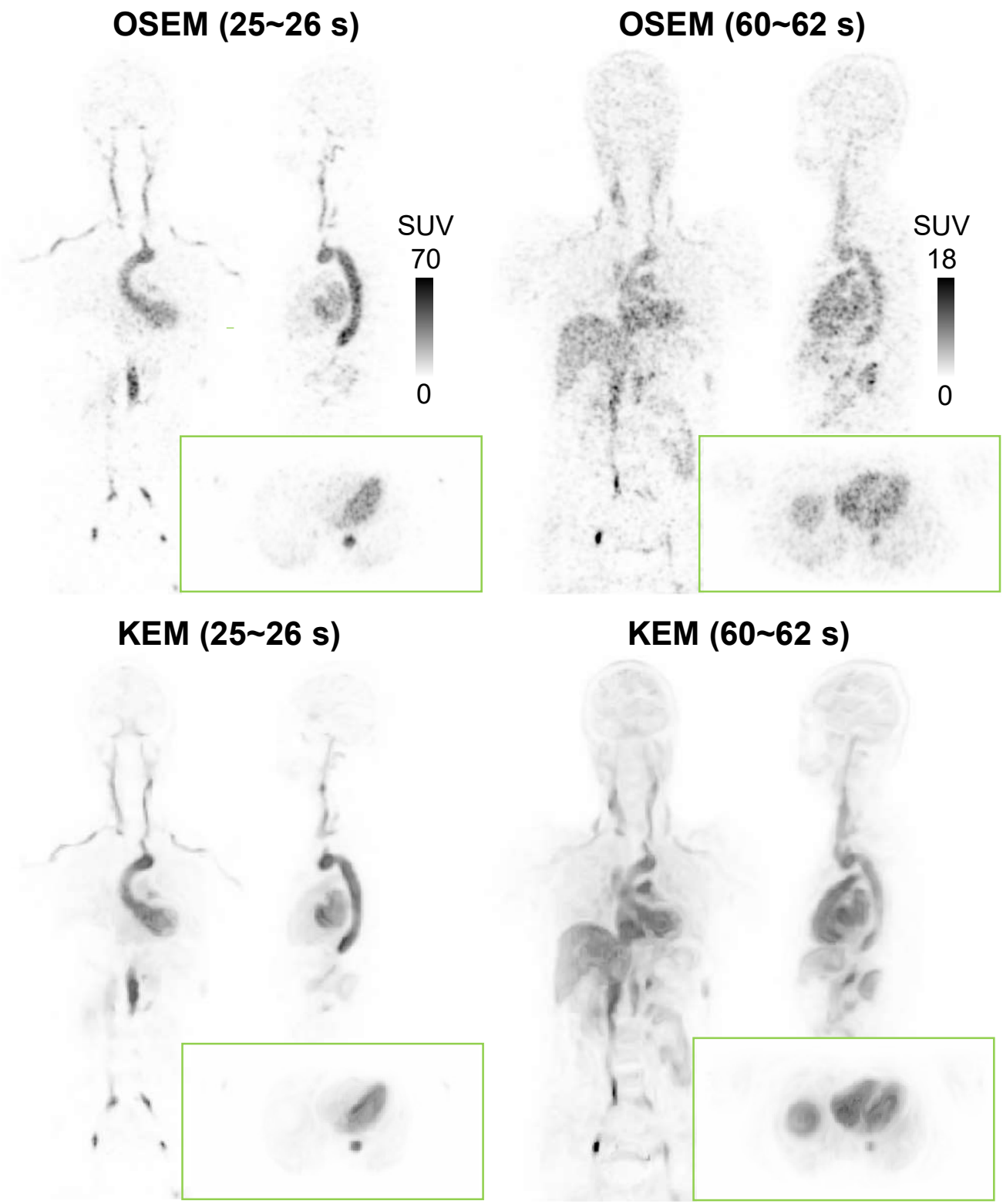

FIGURE 4. Coronal, sagittal, and transaxial image slices of OSEM (top) and kernel-EM (bottom) reconstructions of (left) an early 1-s frame (25~26 s) and (right) a 2-s frame (60-62 s).

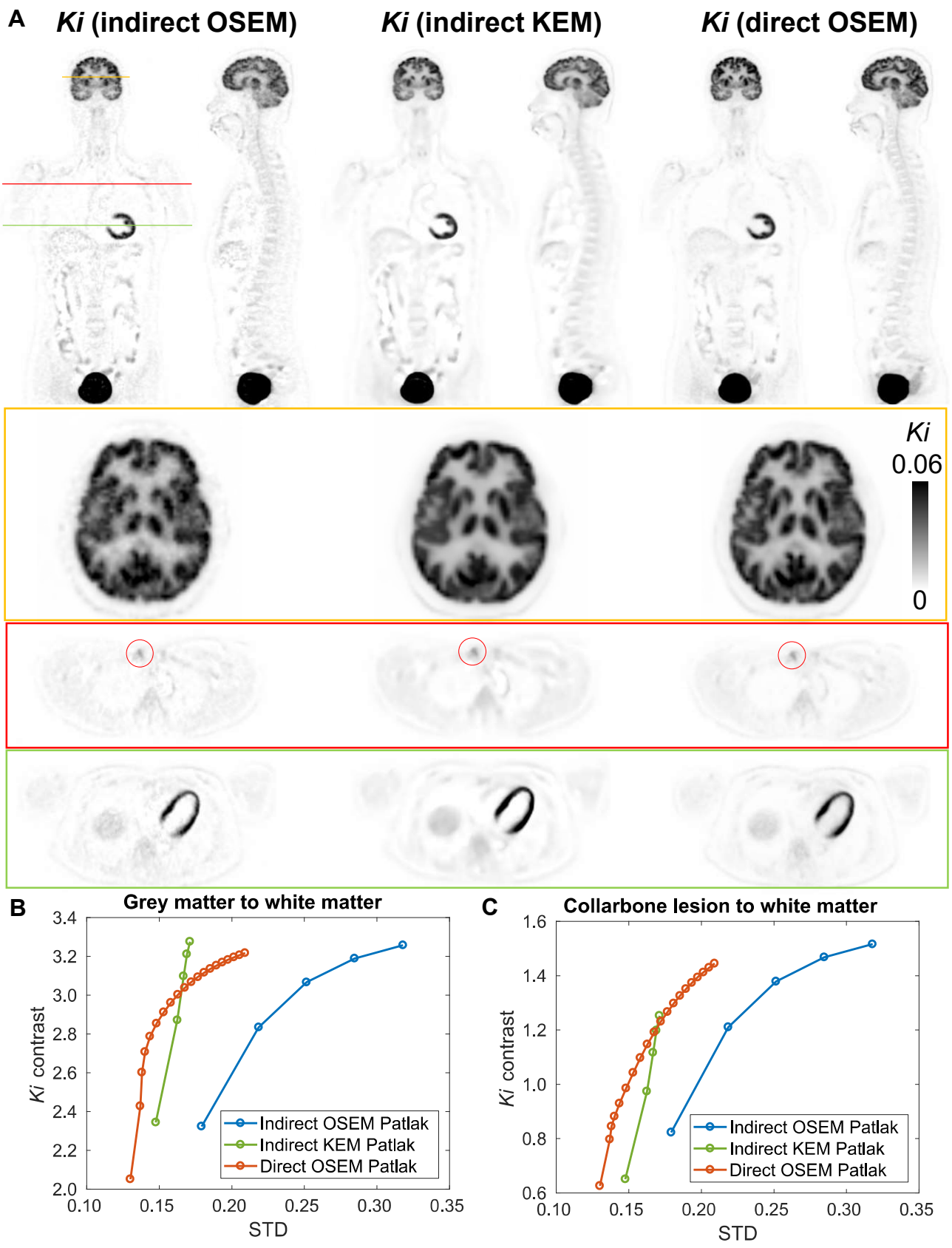

FIGURE 5. (A) Coronal, sagittal, and transaxial image slices of the Patlak slope K_i reconstructed by (left) indirect OSEM Patlak; (middle) indirect Kernel-EM Patlak; (right) direct OSEM Patlak. (B) K_i contrast of

grey matter to white matter versus noise curves. STD was calculated in a large ROI inside the white matter. (C) K_i contrast of a focal uptake lesion (indicated by the red circles) in the collarbone to white matter versus noise curves. STD was calculated using the same white matter ROI as in (B). The *Ki* images are shown in inverse gray scale with the maximum set to 0.06.

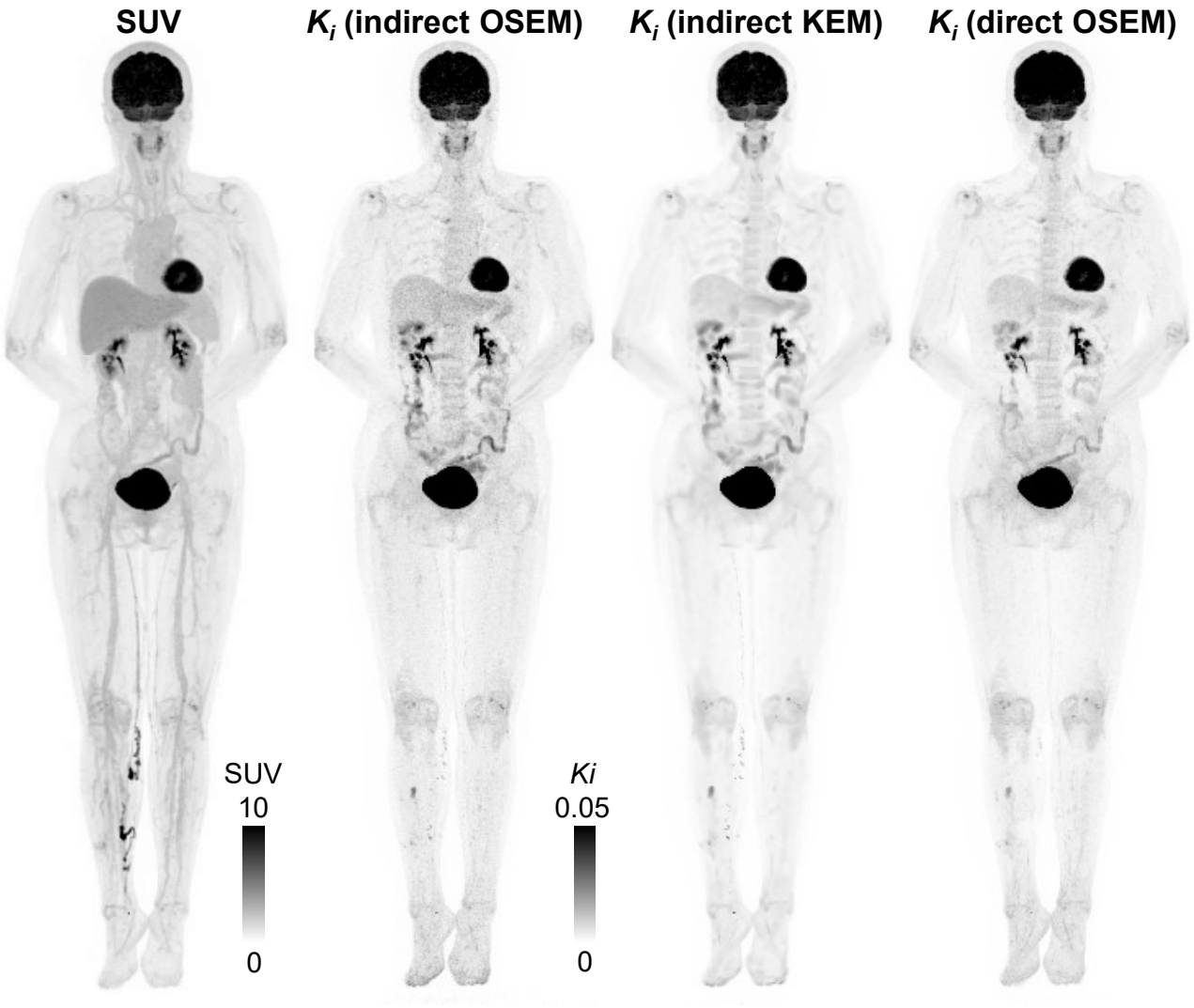

FIGURE 6. Maximum intensity projection (MIP) using last 30 min of data (left to right): SUV; indirect OSEM Patlak slope K_i (3 iterations 10 subsets); indirect kernel-EM Patlak slope K_i (3 iterations 10 subsets); direct OSEM Patlak slope K_i (12 iteration 10 subsets, 10 sub-iterations of parametric update).

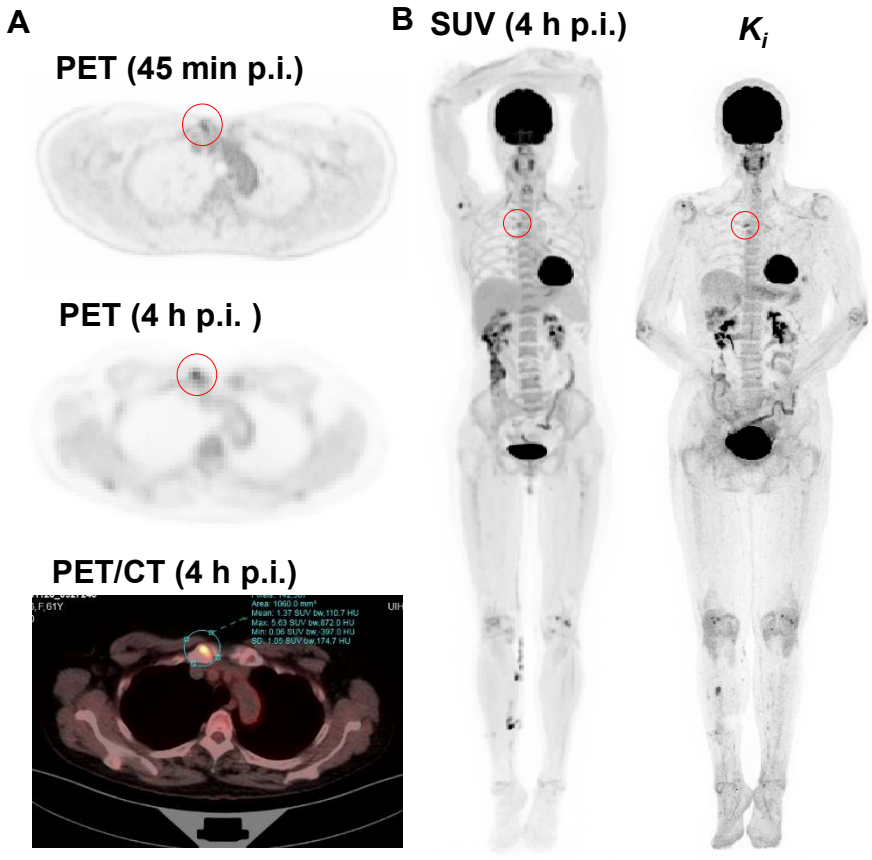

FIGURE 7. Total-body dynamic FDG PET and parametric imaging. (A): Static PET images at 45-min post injection, 4-h post injection, and fused PET/CT image at 4-h post injection to confirm the high FDG uptake at the right sternoclavicular joint, degenerative in nature. Both PET images were obtained with 14-min scan duration. (B): MIPs of OSEM SUV images at 4-h post injection and the indirect Patlak slope K_i image from 30-60 min post-injection scan, respectively. Red circles indicate the high FDG uptake in the right sternoclavicular joint.

TABLE

Table 1. Physical characteristics of the uEXPLORER scanner.

Parameter	Description
Scintillator	Lutetium-yttrium oxyorthosilicate (LYSO)
Photodetectors	Silicon photomultiplier (SiPM)
Crystal pitch and depth	2.85×2.85×18.1 mm
Total number of crystals	564,480
Axial FOV	194 cm
Detector ring diameter	78.6 cm
Transaxial FOV	68.6 cm
TOF resolution	430 ps
Energy resolution	11.7%
Number of LORs	> 90 billion before accounting for TOF
Maximum axial (polar) angle	±57°